Physics of Atomic Nuclei, Vol. 67, No. 8, 2004, pp. 1462–1477. Translated from Yadernaya Fizika, Vol. 67, No. 8, 2004, pp. 1488–1502.

NUCLEI
Theory

Near-Barrier Fusion of Heavy Nuclei: Coupling of Channels

V. I. Zagrebaev* **and V. V. Samarin**

Joint Institute for Nuclear Research, Dubna, Moscow oblast, 141980 Russia

Received April 29, 2003; in final form, November 10, 2003

Abstract—The problem of a quantum-mechanical description of a near-barrier fusion of heavy nuclei that occurs under the conditions of a strong coupling of their relative motion to the rotation of deformed nuclei and to a dynamical deformation of their surfaces is studied. A new efficient method is proposed for numerically solving coupled Schrödinger equations with boundary conditions corresponding to a total absorption of the flux that has overcome a multidimensional Coulomb barrier. The new method involves no limitations on the number of channels that are taken into account and makes it possible to calculate cross sections for the fusion of very heavy nuclei that are used in the synthesis of superheavy elements. A global analysis of the relief of the multidimensional potential surface and of the multichannel wave function in the vicinity of the Coulomb barrier provides a clear interpretation of the dynamics of near-barrier nuclear fusion. A comparison with experimental data and with the results produced by the semiempirical model for taking into account the coupling of channels is performed. © *2004 MAIK "Nauka/Interperiodica".*

INTRODUCTION

The near-barrier fusion of nuclei still attracts the attention of theorists and experimentalists. The dynamics of low-energy fusion is governed by quantum tunneling through a Coulomb barrier, this occurring under conditions where relative motion is strongly coupled to internal degrees of freedom—primarily, to vibrations of nuclear surfaces, the rotation of deformed nuclei, and nucleon transfer [1]. We note that this theoretical problem arises in many realms of physics and chemistry. A considerable improvement of experimental techniques that has been achieved over the past few years in this field provides the possibility of performing precision measurements enabling one to study the details of the subbarrier-fusion process and subtle effects accompanying it (see, for example, [2, 3] and the review article of Dasgupta *et al.* [4]). It is hardly possible to solve the respective quantum-mechanical problem (or its semiclassical analog) exactly. As a result, we still do not have an unambiguous interpretation of experimental data in some cases, despite a rather good understanding of the physics of the process in general. The situation is even worse in predicting subbarrier-fusion cross sections for as-yet-unexplored combinations of heavy nuclei, but such predictions are of paramount importance for planning and performing expensive experiments on the synthesis of superheavy elements.

A few algorithms for numerically solving the set of coupled Schrödinger equations that simulates the coupling of channels in the near-barrier fusion of heavy nuclei have been proposed in recent years. These algorithms rely either on employing some approximate method to diagonalize the coupling matrix at the barrier [5] or on directly constructing a numerical solution to the relevant differential equations [6]. As was shown in [7], colliding heavy nuclei develop rather large dynamical deformations upon the inclusion of realistic forces of nucleus–nucleus interactions, and it is necessary to take into account a large number of excited phonons in order to describe these deformations. Following basically the same line of reasoning as in [6], we developed a new algorithm for solving a set of second-order differential equations. This algorithm makes its possible to avoid imposing any limitations on the number of channels that are taken into account. The second distinctive feature of our approach is that we consider boundary conditions on the incident flux more accurately; that is, we ensure a complete absence of waves reflected from the region behind the barrier. In addition to the barrier penetrability, this makes it possible to calculate the multidimensional wave function itself in the near-barrier region. This function can be used to obtain, via a detailed analysis, deeper insight into the dynamics of multidimensional tunneling. In just the same way as in [6], we do not resort to the linear approximation in the coupling interaction, but, in contrast to [6], we use an explicit (quadrature) method for calculating the matrix elements of the interaction, this method ensuring a preset accuracy independent of the number of channels that are taken into account. This approach is used to analyze the fusion of statically deformed and spherically deformed heavy nuclei. We

*e-mail: valeri.zagrebaev@jinr.ru

compare our results with experimental data and with the results obtained on the basis of the semiempirical model developed for taking into account the coupling of channels in fusion processes.

1. INTERACTION OF DEFORMED NUCLEI

The shape of an axisymmetric deformed nucleus can be described by the formula

$$R(\boldsymbol{\beta},\theta)=\tilde{R}\left(1+\sum_{\lambda\geq 2}\beta_\lambda\sqrt{\frac{2\lambda+1}{4\pi}}P_\lambda(\cos\theta)\right), \tag{1}$$

where $\boldsymbol{\beta}\equiv\{\beta_\lambda\}$ are the dimensionless deformation parameters of multipolarity $\lambda=2,3,...$; P_λ are Legendre polynomials;

$$\tilde{R}=R_0\Bigg[1+\frac{3}{4\pi}\sum_\lambda\beta_\lambda^2 + \frac{1}{4\pi}\sum_{\lambda,\lambda',\lambda''}\sqrt{\frac{(2\lambda'+1)(2\lambda''+1)}{4\pi(2\lambda+1)}} \times(\lambda'0\lambda''0|\lambda0)^2\beta_\lambda\beta'_\lambda\beta''_\lambda\Bigg]^{-1/3}; \tag{2}$$

R_0 is the radius of an equivalent sphere that has the same volume as the deformed nucleus being considered; and $(\lambda'0\lambda''0|\lambda0)$ are Clebsch–Gordan coefficients. The potential energy of the interaction of two deformed nuclei can be written as the sum of the Coulomb and nuclear energies and the deformation energy in the harmonic approximation; that is,

$$V_{12}(r;\boldsymbol{\beta}_1,\theta_1,\boldsymbol{\beta}_2,\theta_2)=V_{\rm C}(r;\boldsymbol{\beta}_1,\theta_1,\boldsymbol{\beta}_2,\theta_2) + V_N(r;\boldsymbol{\beta}_1,\theta_1,\boldsymbol{\beta}_2,\theta_2)+\frac{1}{2}\sum_{i=1}^{2}\sum_\lambda C_{i\lambda}(\beta_{i\lambda}-\beta_{i\lambda}^{\rm g.s.})^2. \tag{3}$$

Here and below, the index $i=1,2$ numbers interacting nuclei; $C_{i\lambda}$ are the stiffness parameters of the nuclear surface; $\theta_{1,2}$ specify the orientations of the symmetry axes of deformed nuclei (see Fig. 1); and $\beta_{i\lambda}^{\rm g.s.}$ are the static deformations of the nuclei.

Disregarding multipole–multipole interactions and retaining terms to second order in the deformations inclusive, we can represent the Coulomb interaction of deformed nuclei in the form

$$V_{\rm C}=Z_1Z_2e^2\times\left[F^{(0)}(r)+\sum_{i=1}^{2}\sum_{\lambda\geq 2}F_{i\lambda}^{(1)}(r)\beta_{i\lambda}Y_{\lambda0}(\theta_i)\right] + Z_1Z_2e^2\sum_{i=1}^{2}\sum_{\lambda'}\sum_{\lambda''}\sum_{\lambda=|\lambda'-\lambda''|}^{\lambda'+\lambda''}F_{i\lambda}^{(2)}(r) \times\sum_{\mu=-\min\{\lambda',\lambda''\}}^{\min\{\lambda',\lambda''\}}\int Y_{\lambda'\mu}^*Y_{\lambda''-\mu}^*Y_{\lambda0}d\Omega \times\beta_{i\lambda'}\beta_{i\lambda''}Y_{\lambda0}(\theta_i)+\ldots, \tag{4}$$

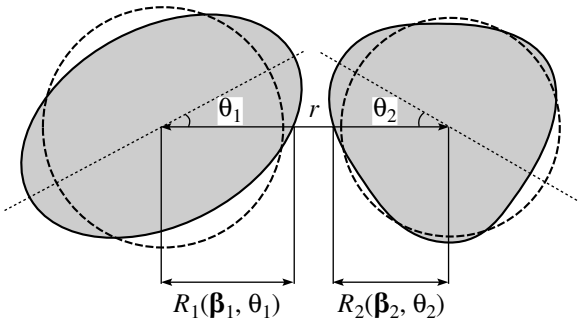

Fig. 1. Relative disposition of two deformed nuclei rotating in the reaction plane ($\boldsymbol{\beta}_i=\{\beta_{i\lambda}\}$).

where $F_\lambda^{(n)}(r)$ are the interaction form factors. For $r>R_1+R_2$, we have

$$F^{(0)}=\frac{1}{r},\quad F_{i\lambda}^{(1)}=\frac{3}{2\lambda+1}\frac{R_i^\lambda}{r^{\lambda+1}},\quad F_{i\lambda=2}^{(2)}=\frac{6}{5}\frac{R_i^2}{r^3},\quad F_{i\lambda=4}^{(2)}=\frac{R_i^4}{r^5}.$$

At smaller values of r, in which case the nuclear surfaces are overlap, the form factors $F_\lambda^{(n)}(r)$ are given by more complicated expressions [8], but this is insignificant for fusion processes, because, here, the position of the Coulomb barrier satisfies the condition $R_{\rm C}^B>R_1+R_2$. In describing the rotation of deformed nuclei, one usually takes into account their quadrupole and (or) hexadecapole deformations. Since the strong inequality $\beta_4\ll 1$ holds as a rule, only $\lambda'=\lambda''=2$ terms are retained in the third term, the values of 2 and 4 being taken for λ.

Short-range nuclear interaction depends on the distance between the nuclear surfaces, which is usually set to the distance along the axis connecting the centers of the nuclei involved, $\xi=r-R_1(\boldsymbol{\beta}_1,\theta_1)-R_2(\boldsymbol{\beta}_2,\theta_2)$, or to the minimum distance between their surfaces (see Fig. 1). This interaction is often approximated by the Woods–Saxon potential $V_{\rm WS}(\xi)=V_0[1+\exp(\zeta/a_V)]^{-1}$, where $\zeta=r-R_V-\Delta R_1-\Delta R_2$, $\Delta R_1=R_1(\boldsymbol{\beta}_1,\theta_1)-R_1$, and $\Delta R_2=R_2(\boldsymbol{\beta}_2,\theta_2)-R_2$. It should be recalled that, for the Woods–Saxon potential, the interaction range $R_V=r_0^V(A_1^{1/3}+A_2^{1/3})$ usually does not coincide with the sum of the radii of the nuclei themselves, so that r_0^V is an additional independent parameter. As an alternative possibility, one can describe nuclear

interaction in terms of the "proximity" potential [9]

$$V_{\rm prox}(\xi) = 4\pi\gamma b P_{\rm sph}^{-1}\Phi(\xi/b), \qquad (5)$$

where $\Phi(\xi/b)$ is a universal dimensionless form factor; b is a parameter that characterizes the surface-layer thickness (about 1 fm); $\gamma = \gamma_0(1 - 1.7826I^2)$, with $\gamma_0 = 0.95$ MeV fm^{-2} being the surface-tension coefficient and I being given by $I = (N - Z)/A$; $\xi = r - R_1(\boldsymbol{\beta}_1, \theta_1) - R_2(\boldsymbol{\beta}_2, \theta_2)$; and $P_{\rm sph} = 1/\bar{R}_1 + 1/\bar{R}_2$ with $\bar{R}_i = R_i[1 - (b/R_i)^2]$. This interaction is the most sensitive to the choice of matter radii for nuclei. The most realistic results are obtained if use is made of $r_0 \approx 1.16$ fm for the radii of heavy nuclei ($A > 40$) and of $r_0 \approx 1.22$ fm for the radii of $A \sim 16$ nuclei. The most important advantage of the proximity potential is that it is universal in the sense that this potential features no adjustable parameters like V_0, r_0^V, or a_V.

The attraction of two nuclear surfaces also depends on their curvature [9, 10]—that is, on the area of touching surfaces. Usually, this is taken into account by replacing the quantity $P_{\rm sph}$ in (5) by the expression

$$P(\boldsymbol{\beta}_1, \theta_1, \boldsymbol{\beta}_2, \theta_2) = \left[(k_1^{||} + k_2^{||})(k_1^{\perp} + k_2^{\perp})\right]^{1/2}, \quad (6)$$

where $k_i^{||,\perp}$ are the principal parameters of the local curvature of the surfaces of interacting nuclei (see, for example, [11]). For spherical nuclei, $k_i^{||,\perp} = R_i^{-1}$ and $P = P_{\rm sph}$. In the case of dynamical deformations along the axis connecting the centers of the two nuclei ($\theta_1 = \theta_2 = 0$)—it is realized in slow collisions of dynamically deformable nuclei—the local curvature can be found explicitly (see Appendix 1), which yields

$$P(\boldsymbol{\beta}_1, \theta_1 = 0, \boldsymbol{\beta}_2, \theta_2 = 0) \qquad (7)$$
$$= \sum_{i=1,2} \frac{1}{\tilde{R}_i}\left(1 + \sum_{\lambda\geq 2}\sqrt{\frac{2\lambda+1}{4\pi}}\beta_{i\lambda}\right)^{-2}$$
$$\times \left(1 + \sum_{\lambda\geq 2}(1 + \eta(\lambda))\sqrt{\frac{2\lambda+1}{4\pi}}\beta_{i\lambda}\right),$$

where $\eta(\lambda) = 3 \cdot 4 \cdots (\lambda + 1)/(\lambda - 1)!$. For rotating deformed nuclei, it is necessary, in principle, to take into account the difference of the shortest distance ξ_S between the surfaces and the distance ξ calculated along the central line (see Fig. 1). For realistic deformations, however, the resulting effect of taking into account the inequality of ξ_S and ξ in calculating the interaction potentials and fusion cross sections is quite small in relation to the effect of the change in the curvature ($P \neq P_{\rm sph}$) [12].

Formally, expression (6) can vanish at some negative values of the deformation (the touching of two planar surfaces). This unphysical effect arises because of the disregard of finite dimensions of the areas of touching nuclear surfaces and indicates that it is necessary to go over to a more precise approximation at large negative deformations. The main contribution to the nucleus–nucleus potential comes from the interactions of the most closely spaced nucleons, whose number, albeit depending on the local curvature of the surfaces, is always finite. Thus, we see that, instead of merely substituting the quantity P for $P_{\rm sph}$ in (5), it would be more correct, for the short-range nucleus–nucleus interaction, to employ the expression $V_N = G(\boldsymbol{\beta}_1, \theta_1, \boldsymbol{\beta}_2, \theta_2)V_N^0(r; \boldsymbol{\beta}_1, \theta_1, \boldsymbol{\beta}_2, \theta_2)$, where $V_N^0(r; \boldsymbol{\beta}_1, \boldsymbol{\theta}_1, \boldsymbol{\beta}_2, \theta_2)$ is the interaction that was calculated with allowance for the deformations of the nuclei and their relative orientation but without taking into account the change in the curvature of the surfaces, while $G(\boldsymbol{\beta}_1, \theta_1, \boldsymbol{\beta}_2, \theta_2)$ is a geometric factor that takes into account the change in the number of interacting nucleons that occur in the closely spaced layers of the two nuclei in relation to the case of spherical surfaces. In Appendix 2, we present a derivation of an approximate expression for the geometric factor $G(\boldsymbol{\beta}_1, \theta_1, \boldsymbol{\beta}_2, \theta_2)$, which plays a significant role at not very small deformations.

The nuclear-surface-deformation stiffness C_λ can be found from the experimental value of the probability $B(E\lambda)$ of an electromagnetic transition involving the excitation of one vibrational quantum [13]. Specifically, we have

$$C_\lambda = (2\lambda + 1)\frac{\varepsilon_\lambda}{2\langle\beta_\lambda^0\rangle^2}, \qquad (8)$$

where $\varepsilon_\lambda = \hbar\omega_\lambda$ is the energy of a vibrational quantum and

$$\langle\beta_\lambda^0\rangle = \frac{4\pi}{3ZR_0^\lambda}\left[\frac{B(E\lambda)}{e^2}\right]^{1/2}$$

is the root-mean-square value of the total deformation for zero-point vibrations. If there are no relevant experimental data, the parameters of nuclear-surface vibrations can be determined on the basis of the liquid-drop model [13]; that is,

$$C_\lambda^{\rm LD} = \gamma_0 R_0^2(\lambda - 1)(\lambda + 2) - \frac{3}{2\pi}\frac{Ze^2}{R_0}\frac{(\lambda - 1)}{(2\lambda + 1)}, \qquad (9a)$$

$$D_\lambda^{\rm LD} = \frac{3}{4\pi}\frac{Am_N R_0^2}{\lambda}, \quad \varepsilon_\lambda = \hbar\sqrt{\frac{C_\lambda^{\rm LD}}{D_\lambda^{\rm LD}}}, \qquad (9b)$$

where $D_\lambda^{\rm LD}$ is the mass parameter, A is the number of nucleons in the nucleus being considered, and m_N

is the nucleon mass. We note that, in many cases (especially for magic nuclei), the liquid-drop model yields, for the parameters of surface vibrations, values that differ from their experimental counterparts considerably. For the ensuing calculations (we also bear in mind the possibility of parallel calculations employing the equations of classical mechanics), it is convenient to go over to the absolute values of the nuclear deformation, $s_\lambda = \sqrt{(2\lambda+1)/4\pi}R_0\beta_\lambda$. In this case, the potential energy of a specific vibration can be represented in the form $c_\lambda s_\lambda^2/2$, where

$$c_\lambda = C_\lambda \left(\frac{2\lambda+1}{4\pi}R_0^2\right)^{-1} = \frac{\hbar\omega_\lambda}{2\langle s_\lambda^0\rangle^2}$$

and

$$\langle s_\lambda^0\rangle = \frac{R_0}{\sqrt{4\pi}}\langle\beta_\lambda^0\rangle,$$

while the mass parameter is determined from the relation $\omega_\lambda = \sqrt{c_\lambda/d_\lambda}$; within the liquid-drop model, we have

$$d_\lambda^{\mathrm{LD}} = D_\lambda^{\mathrm{LD}}\left(\frac{2\lambda+1}{4\pi}R_0^2\right)^{-1} = \frac{3}{\lambda(2\lambda+1)}Am_N.$$

The two-dimensional interaction potential (3) for the spherical nucleus ^{16}O and the deformed nucleus ^{154}Sm ($\beta_2^{\mathrm{g.s.}} = 0.3$, $\beta_4^{\mathrm{g.s.}} = 0.1$) is displayed in Fig. 2*a* versus the relative orientation of these two nuclei. The potential of interaction of two spherical nuclei ^{40}Ca and ^{90}Zr versus their dynamical quadrupole deformation is shown in Fig. 2*b* according to the calculations with the parameters of the liquid-drop model (for the sake of simplicity, it was assumed here that the deformation energy of the nuclei is proportional to their masses; thus, only one parameter $\beta = \beta_1 + \beta_2$ was used instead of two dynamical-deformation parameters β_1 and β_2). In order to simulate the nuclear part of the interaction, we used the Woods–Saxon potential with parameters $V_0 = -105$ MeV, $r_0^V = 1.12$ fm, and $a_V = 0.75$ fm in the first case and the proximity potential with parameter $r_0^i = 1.16$ for the nuclear radii in the second case. The figures clearly demonstrate the multidimensional character of the potential of the nucleus–nucleus interaction and of the potential barrier itself, which, as is readily seen, cannot be characterized by its height B alone; it would be more correct to consider some continuous distribution $F(B)$ of barriers (see below).

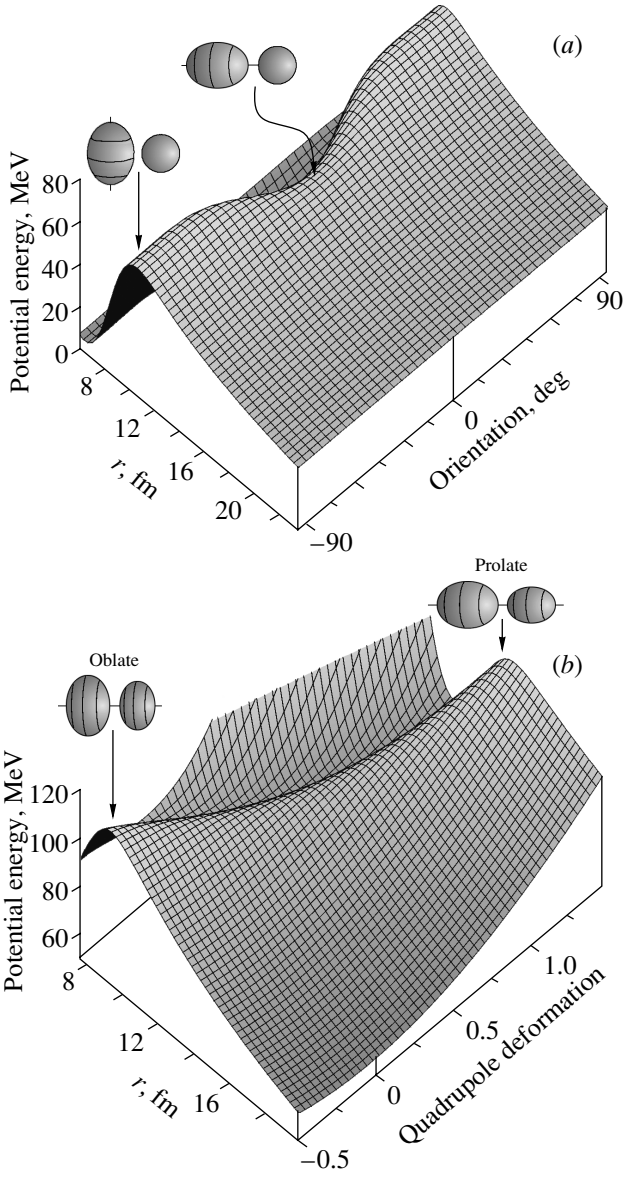

Fig. 2. (*a*) Interaction potential for the ^{16}O and ^{154}Sm ($\beta_2^{\mathrm{g.s.}} = 0.3, \beta_4^{\mathrm{g.s.}} = 0.1$) nuclei versus the distance and relative orientation. (*b*) Potential energy of the interaction of the spherical nuclei ^{40}Ca and ^{90}Zr versus the distance and their dynamical quadrupole deformation.

2. SET OF COUPLED EQUATIONS AND BOUNDARY CONDITIONS

For two deformed nuclei rotating in the reaction plane, the Hamiltonian can be represented in the form

$$H = -\frac{\hbar^2\nabla_r^2}{2\mu} + V_{\mathrm{C}}(r;\boldsymbol{\beta}_1,\theta_1,\boldsymbol{\beta}_2,\theta_2) \qquad (10)$$

$$+ V_N(r;\boldsymbol{\beta}_1,\theta_1,\boldsymbol{\beta}_2,\theta_2) + \sum_{i=1,2}\frac{\hbar^2\hat{I}_i^2}{2\Im_i}$$

$$+ \sum_{i=1,2}\sum_{\lambda\geq 2}\left(-\frac{\hbar^2}{2d_{i\lambda}}\frac{\partial^2}{\partial s_{i\lambda}^2} + \frac{1}{2}c_{i\lambda}s_{i\lambda}^2\right),$$

where μ is the reduced mass of these two nuclei and $\hat{I}_i$ and $\Im_i$ are, respectively, the operator of the angular momentum and the moment of inertia of the ith nucleus. In the algorithm developed for solving the

quantum set of coupled equations, we assumed the independence of vibrations having different multipole orders (not greater than two in each nucleus) and also disregarded the coupling of rotations and vibrations, considering them separately. It turned out that the algorithm used here enabled one to solve, within a reasonable time, a rather large number of coupled equations (about 300 for each partial wave with a computer having 128 Mbytes of random-access memory), this providing the possibility of dispensing, in the following, with approximations where different excitations are considered to be independent. The maximum number of channels whose coupling can be taken into account in the code used is estimated by the formula $N_\nu \sim 500\sqrt{M/N_r}$, where N_r is the number of nodes of the mesh in the radial direction (r) and M is the computer random-access memory in megabytes. In solving the quantum problem in question, we employ the so-called isocentrifugal approximation [14], which consists in disregarding the intrinsic spins of nuclei against the orbital angular momentum of relative motion, this orbital angular momentum being assumed to be identical in all channels (conserved quantum number). This approximation makes it possible to reduce severalfold the dimensionality of the set of differential equations that is to be solved.

Expanding, in terms of partial waves, the total wave function for the system being considered as

$$\Psi_{\mathbf{k}}(r,\vartheta,\boldsymbol{\alpha}) = \frac{1}{kr}\sum_{l=0}^{\infty} i^l e^{i\sigma_l}(2l+1)\chi_l(r,\boldsymbol{\alpha})P_l(\cos\vartheta) \tag{11}$$

and substituting this expansion into the Schrödinger equation, we arrive at the following set of coupled equations:

$$\frac{\partial^2}{\partial r^2}\chi_l(r,\boldsymbol{\alpha}) - \left\{\frac{l(l+1)}{r^2} + \frac{2\mu}{\hbar^2}\right. \tag{12}$$
$$\left.\times\left[E - V(r,\boldsymbol{\alpha}) - \hat{H}_{\rm int}(\boldsymbol{\alpha})\right]\right\}\chi_l(r,\boldsymbol{\alpha}) = 0.$$

Here, α stands for intrinsic variables (deformation parameters or rotation angles), $\hat{H}_{\rm int}(\boldsymbol{\alpha})$ is the Hamiltonian corresponding to these variables, E is the energy of colliding nuclei in the c.m. frame, and $V(r,\boldsymbol{\alpha}) = V_{\rm C}(r,\boldsymbol{\alpha}) + V_N(r,\boldsymbol{\alpha})$. At all values of r, with the exception of those in the region where the nuclei involved are in contact (see below), the function $\chi_l(r,\boldsymbol{\alpha})$ is expanded in the total set of eigenfunctions of the Hamiltonian $\hat{H}_{\rm int}(\boldsymbol{\alpha})$,

$$\chi_l(r,\boldsymbol{\alpha}) = \sum_\nu y_{l,\nu}(r)\varphi_\nu(\boldsymbol{\alpha}), \tag{13}$$

while the radial channel wave functions $y_{l,\nu}(r)$ satisfy a set of second-order ordinary differential equations that, in the following, is solved numerically,

$$y''_{l,\nu} - \left\{\frac{l(l+1)}{r^2} + \frac{2\mu}{\hbar^2}\left[E_\nu - V_{\nu\nu}(r)\right]\right\} y_{l,\nu} \tag{14}$$
$$- \sum_{\mu\neq\nu}\frac{2\mu}{\hbar^2}V_{\nu\mu}(r)y_{l,\mu} = 0.$$

Here, $E_\nu = E - \varepsilon_\nu$, where ε_ν is the excitation of the nuclei in the channel ν, and $V_{\nu\mu}(r) = \langle\varphi_\nu|V(r,\boldsymbol{\alpha})|\varphi_\mu\rangle$ is the channel-coupling matrix.

In a low-energy collision of not very heavy nuclei, nuclei that have overcome the Coulomb barrier undergo fusion (that is, form a compound nucleus) with a probability close to unity as soon as their surfaces come into contact. In this case, the fusion cross section can be measured by examining the total yield of evaporated residues and fragments originating from compound-nucleus fission. In formulating boundary conditions for Eqs. (14), it is therefore usually assumed that the flux in the region behind the Coulomb barrier is fully absorbed; that is, it does not undergo reflection. For this purpose, we require that, for $r < R_{\rm fus}$, the functions $\chi_l(r,\boldsymbol{\alpha})$ have the form of converging waves and not involve components corresponding to waves reflected from the region $0 \le r \le R_{\rm fus}$. For $R_{\rm fus}$, Hagino *et al.* [6] took the point of minimum of the potential

$$V_{\rm eff}(r) = V(r,0) + \frac{\hbar^2}{2\mu}\frac{l(l+1)}{r^2},$$

which, for $r \le R_{\rm fus}$, is replaced by the quantity $V_{\rm eff}(R_{\rm fus})$, the coupling of channels being switched off at the point $r = R_{\rm fus}$. The set of coupled Eqs. (14) then decouples, and we can easily choose their solutions corresponding to converging waves ($\exp(-iqr)$). However, an abrupt charge in the channel-coupling interaction, whose strength reaches maximum values in this region, may in principle lead to an additional unphysical reflection from the sphere $r = R_{\rm fus}$ and, hence, to a significant distortion of the total wave function in the barrier region.

In order to remove this effect, we will first modify the phenomenological potential $V(r,\boldsymbol{\alpha})$ of nucleus–nucleus interaction in the nuclear-surface-overlap region $r \le R_{\rm cont}(\boldsymbol{\alpha}) \le R_1(\boldsymbol{\beta}_1,\theta_1) + R_2(\boldsymbol{\beta}_2,\theta_2)$, rendering it independent of r in this region, $V(r \le R_{\rm cont},\boldsymbol{\alpha}) = V(R_{\rm cont},\boldsymbol{\alpha})$. For $R_{\rm cont}(\boldsymbol{\alpha})$, we will take the minimum of two distances from $r = 0$, that to the point of minimum of the potential $V(r,\boldsymbol{\alpha})$ and that to the point at which the nuclear surfaces touch each other. The boundary-value problem for Eqs. (14) will be considered over the interval $(R_{\rm min}, R_{\rm max})$, where $R_{\rm max} \gg R_1 + R_2$, $R_{\rm min} \le$

$\min\{R_{\rm cont}(\boldsymbol{\alpha})\}$ in the case of rotations, and $R_{\min} \le R_{\rm cont}(-\sqrt{M_1}\langle\boldsymbol{\beta}_1^0\rangle, -\sqrt{M_2}\langle\boldsymbol{\beta}_2^0\rangle)$ in the case of vibrations; here, M_1 and M_2 are the maximum numbers of channels that are taken into account and $\langle\boldsymbol{\beta}_1^0\rangle$ and $\langle\boldsymbol{\beta}_2^0\rangle$ are the vectors of the root-mean-square values of the deformation parameters. The centrifugal potential is also replaced by the constant value

$$U_l = \frac{\hbar^2}{2\mu}\frac{l(l+1)}{R_s^2}$$

for $r < R_s$, where, for $R_s > R_{\min}$, we take the minimum of two distances from $r = 0$, that to the point of minimum of the effective potential for spherical nuclei, $V_{\rm eff}(r)$, and that to the point at which the spherical nuclei touch each other. The choice of $R_{\min}$ is rather arbitrary. It is only of importance that it lie in the region behind the Coulomb barrier: $R_{\min} < R_B(\boldsymbol{\alpha})$. The second item to be mentioned here is that, in formulating boundary conditions at the point $r = R_{\rm fus} = R_s \le R_{\rm cont}$, from which we begin integrating the set of differential Eqs. (14), we will make use of an exact solution to these equations in the region $r \le R_{\rm fus}$. This solution can easily be found if all coefficients in these equations are constant.

For $r \le R_{\rm fus}$, we will further perform the linear transformation

$$y_{l,\nu}(r) = \sum_n Y_{l,n}(r)A_{n,\nu}, \qquad (15)$$

which diagonalizes the matrix $W_{\nu\mu} = V_{\nu\mu}(R_{\rm fus}) + \varepsilon_\nu\delta_{\nu\mu}$, so that $\{A^{-1}WA\}_{nm} = \tilde{W}_{nn}\delta_{nm}$. The new functions $Y_{l,n}(r)$ satisfy the independent equations

$$Y''_{l,n} + K^2_{l,n}Y_{l,n} = 0, \quad K^2_{l,n} = \frac{2\mu}{\hbar^2}[E - \tilde{W}_{nn} - U_l]. \qquad (16)$$

In open channels, the particular solutions $Y_{l,n}(r) = N_{l,n}\exp(-iK_{l,n}r)$ satisfying these equations and the conditions $Y'_{l,n}(r) = -iK_{l,n}Y_{l,n}(r)$ correspond to a flux toward the interior of the nucleus. From the linear transformation (15), we obtain boundary conditions for the sought channel wave functions $y_{l,\nu}(r)$ at $r \le R_{\rm fus}$; that is,

$$y'_{l,\nu}(r) = \sum_n Y'_{l,n}(r)A_{n,\nu} = \sum_\mu C_{\nu\mu}y_{l,\mu}(r), \qquad (17)$$

where

$$C_{\nu\mu} = -i\sum_n A_{n,\nu}K_{l,n}(A^{-1})_{n,\mu}.$$

The values $\tilde{W}_{nn}$ are the eigenvalues of the matrix $W_{\nu\mu}$, while the matrix $A_{n\nu}$ is composed of its normalized eigenvectors. They can be found explicitly by applying the so-called QR method [15].

At large distances, the wave function satisfies standard boundary conditions in the form of an incident and a diverging wave in the elastic channel $\nu = 0$ and in the form of diverging waves in all other channels. For partial wave functions in open channels, this corresponds to the condition

$$y_{l,\nu}(r \to \infty) = \frac{i}{2}\left[h_l^{(-)}(\eta_\nu, k_\nu r)\delta_{\nu 0} - \left(\frac{k_0}{k_\nu}\right)^{1/2} S^l_{\nu 0}h_l^{(+)}(\eta_\nu, k_\nu r)\right], \qquad (18)$$

where $k_\nu^2 = (2\mu/\hbar^2)E_\nu$, $\eta_\nu = k_\nu Z_1 Z_2 e^2/(2E_\nu)$ is the Sommerfeld parameter, $h_l^{(\pm)}(\eta_\nu, k_\nu r)$ are the Coulomb partial wave functions whose asymptotic behavior is $\exp(\pm ix_{l,\nu})$, $x_{l,\nu} = k_\nu r - \eta_\nu \ln 2k_\nu r + \sigma_{l,\nu} - l\pi/2$, $\sigma_{l,\nu} = \arg\Gamma(l+1+i\eta_\nu)$ is the Coulomb phase shift, and $S^l_{\nu 0}$ is the partial-wave scattering matrix. Eliminating the unknown quantities $S^l_{\nu 0}$ in (18), we obtain, at large distances, boundary conditions of the third kind,

$$\left[y_{l,\nu}\frac{dh_l^{(+)}}{dr} - \frac{dy_{l,\nu}}{dr}h_l^{(+)}\right]_{r=R_{\max}} = k_0\delta_{\nu 0}, \qquad (19)$$

which, together with the conditions in (17), are sufficient for numerically solving the set of coupled second-order differential Eqs. (14). For closed channels ($E_\nu < 0$), there arise similar expressions involving Coulomb functions of an imaginary argument.

In specific calculations, the boundary conditions (18) are actually employed at some finite radius, $R_{\max} \sim 30$–40 fm. For very heavy nuclei, which are characterized by large values of Z, the presence of the weakly decreasing ($\sim r^{-3}$) channel-coupling Coulomb interaction (4) results in that, at $r = R_{\max}$, the nuclei involved are already in an excited state, so that it is illegitimate to use the boundary conditions (19) at this point. The physical meaning of more correct boundary conditions is quite obvious. The Coulomb repulsion leads to negative dynamical deformations (oblate nuclei) and to a preferable side-to-side orientation of rotating quadrupolly deformed nuclei. There exist two methods for quantitatively solving this problem. In the region $r \ge R_{\max}$, one can consider a smaller number of coupled channels and solve the problem numerically within the interval $R_{\max} \le r \le R_{\rm MAX}$ by using, for example, the approximation of weak channel coupling. Taking $R_{\rm MAX}$ to be about 300 fm and imposing the "reflection-free" boundary conditions for $r \le R_{\max}$, we can find the values of all channel wave functions at this point and employ thereupon these values instead of the boundary conditions (19) in numerically solving the

full set of Eqs. (14) within the interval $R_{\rm fus} \le r \le R_{\max}$. An alternative method for deriving more correct boundary conditions at the point $r = R_{\max}$ is that of constructing an analytic solution to the problem under study in the adiabatic approximation, which assumes that, with the highest probability, the system in question moves along the bottom of the multidimensional potential surface. In this case, we can find the ground state of the system for the Hamiltonian $H_{\rm int}(\boldsymbol{\alpha}) + V(R_{\max}\boldsymbol{\alpha})$ and expand thereupon this state in the functions $\varphi_\nu(\boldsymbol{\alpha})$. The resulting expansion coefficients will yield the amplitudes of converging waves for $r \le R_{\max}$ in all channels, not only in the $\nu = 0$ channel, as is indicated in relation (18). The results of our analysis of effects of long-range Coulomb excitation in processes of near-barrier nuclear fusion will be reported in a dedicated publication.

The channel-coupling interaction $V(r, \boldsymbol{\alpha})$ can be broken down into the slowly decreasing Coulomb component (4) and the fast decreasing nuclear component; accordingly, the channel-coupling matrix has the form $V_{\nu\mu}(r) = V^{\rm C}_{\nu\mu}(r) + V^N_{\nu\mu}(r)$. The Coulomb component of the channel-coupling matrix is known in an explicit form (see, for example, [6]). In order to take explicitly into account nonlinear effects of nuclear interaction, methods of matrix algebra were applied in [6] in calculating the matrix elements of $V^N_{\nu\mu}(r)$. As a matter of fact, this approach is equivalent to expanding the function $V^N(r, \boldsymbol{\alpha})$ in a series in powers of $\boldsymbol{\alpha}$ to the Mth order inclusive, where M is the maximum number of excited states that are taken into account. In the present study, the quantities $V^N_{\nu\mu}(r)$ at each value of r are calculated explicitly with the aid of the Gauss (for rotations) and Gauss–Hermite (for vibrations) quadrature formulas of order N. If, in the expansion of the function $V^N(r, \boldsymbol{\alpha})$ in powers of $\boldsymbol{\alpha}$, one retains terms to the kth order inclusive, it is sufficient, for obtaining precise values of the matrix elements, to use an order $N \ge M + (k+1)/2$ in each degree of freedom. Our experience has revealed that the choice of $N = M + 10$ for rotations and $N = M + 6$ for vibrations is sufficient for obtaining quite an accurate result if use is made of realistic nucleus–nucleus interactions.

The fusion cross section is determined by the ratio of the absorbed to the incident flux; that is,

$$\sigma_{\rm fus}(E) = \frac{\pi}{k_0^2}\sum_{l=0}^{\infty}(2l+1)T_l(E), \qquad (20)$$

where

$$T_l(E) = \sum_\nu \frac{j_{l,\nu}}{j_0} \qquad (21)$$

are the partial-wave barrier-penetrability coefficients. Here,

$$j_{l,\nu} = -i\frac{\hbar}{2\mu}\left(y_{l,\nu}\frac{dy^*_{l,\nu}}{dr} - y^*_{l,\nu}\frac{dy_{l,\nu}}{dr}\right)\Big|_{r\le R_{\rm fus}}$$

is the partial-wave flux in the channel ν and $j_0 = \hbar k_0/\mu$. In the fusion of heavier nuclei (especially for symmetric combinations), the probability that a compound nucleus is formed after the surfaces of colliding nuclei have come into contact is less than unity because of quasifission processes [16]. It is very difficult to calculate this probability [17], and this presents a problem in itself, which is beyond the scope of the algorithm considered here. For such systems, the cross section calculated by formula (20) will correspond to the so-called capture cross section, which is equal to the sum of the fusion cross section and the quasifission cross section.

3. CONSTRUCTING A NUMERICAL SOLUTION TO OUR SET OF COUPLED EQUATIONS

For a finite number of channel functions, the set of ordinary differential Eqs. (14) supplemented with the boundary conditions (17) and (19) forms a mixed boundary-value problem. In order to solve it numerically, we introduce a mesh and specify mesh functions at its nodes as

$$r_j = r_0 + jh, \quad y^j_{l,\nu} = y_{l,\nu}(r_j), \qquad (22)$$
$$j = 0, 1, \ldots, J, \quad r_0 = R_{\rm fus} - 2h.$$

The boundary conditions involving the first derivative are approximated in terms of a two-point difference scheme. For open channels, the condition in (19) leads to the relation

$$y_{l,\nu}(r_J) = \tau y_{l,\nu}(r_{J-1}) - \zeta, \qquad (23)$$
$$\tau = \frac{2+h\gamma}{2-h\gamma}, \quad \zeta = \frac{2hk_\nu\delta_{\nu 0}}{(2-h\gamma)h^{(+)}_l(\eta_\nu, k_\nu r_{J-1/2})},$$
$$\gamma = \frac{dh^{(+)}_l(\eta_\nu, k_\nu r_{J-1/2})/dr}{h^{(+)}_l(\eta_\nu, k_\nu r_{J-1/2})}.$$

Similar formulas are obtained for closed channels as well. The boundary condition (17) yields the matrix relation

$$y_{l,\nu}(r_0) = \sum_\mu \Theta_{\nu\mu}y_{l,\mu}(r_1), \quad \Theta = D^{-1}F, \qquad (24)$$
$$D_{\nu\mu} = \delta_{\nu\mu} + \frac{h}{2}C_{\nu\mu}, \quad F_{\nu\mu} = \delta_{\nu\mu} - \frac{h}{2}C_{\nu\mu}.$$

In order to approximate differential equations by finite-difference equations, use is usually made of Numerov's method, which has been successfully tested

many times (see, for example, [18]) and which is based on a three-point approximation of the second derivative. As a matter of fact, this method ensures an $O(h^4)$ approximation at one step in solving the Schrödinger equation along the mesh. Numerov's method was used in [6] as well. The finite-difference equations obtained by writing the differential Eqs. (14) at internal nodes of the mesh and taken together with the boundary conditions (23) and (24) for the pair of extreme nodes form a set of linear equations whose matrix is banded. In order to reduce the number of nonzero matrix elements in approximating the second derivative, we employ, instead of Numerov's method, the three-point finite-difference scheme

$$y''(r_j) = h^{-2}(y^{j-1} - 2y^j + y^{j+1}) + O(h^2), \quad (25)$$

the half-width of the resulting matrix appearing to be one-half as great as that in Numerov's method. Although the finite-difference scheme (25) ensures an $O(h^2)$ approximation in solving the Schrödinger equation, this is quite sufficient for deriving a solution to a high precision. It should be noted that the error in numerically solving the boundary-value problem (14) arises and is accumulated not only because of a finite-difference approximation of the derivatives involved but also in solving the set of linear equations. For $h \to 0$, the first component of this error decreases, while the second increases because of an increase in the number of equations and in the number of required computational operations. As a result, the total error first decreases and then begins to increase as the step is reduced. The testing of the two algorithms revealed that the accuracy of Numerov's scheme itself is, as a rule, excessive and that, if use is made of a multisweep algorithm in solving the boundary-value problem, its resulting error may exceed the error of the method based on the scheme in (25).

Since modern computers make it possible to save the matrix in random-access memory entirely, we will use the Gauss reduction method to solve our set of linear equations directly and to determine the values of $y_{l,\nu}(r_j)$ at the nodes of the mesh. The main advantage of the approach based on the Gauss reduction method is its high stability in calculations involving a finite number of digital places. A scheme consisting of one direct and one inverse sweep seems preferable to a scheme involving a few sweeps in one direction that are followed by solving a set of linear equations for determining arbitrary constants. In the latter case, the error can increase because of the loss of the required accuracy of the decreasing solution in the classically inaccessible region, this being especially important in solving problems where there are two turning points. The use of the Gauss reduction method in order to solve the set of linear equations directly enabled us to increase, in relation to the possibility presently realized in the CCFULL code [6], the number of channels that are taken into account almost by an order of magnitude. This is especially important in the case where a few degrees of freedom are excited in both nuclei and for avoiding unphysical nuclear-deexcitation effects associated with stringent constraints on the number of coupled channels that are taken into account. Owing to the storage of all values of $y_{l,\nu}(r_j)$ in computer memory, one can also easily reconstruct the multichannel wave functions (11) and (13) themselves and, hence, obtain deeper and clearer insights into the dynamics of penetration through a multidimensional potential barrier (see below).

4. DISTRIBUTION WITH RESPECT TO BARRIERS AND SEMIEMPIRICAL MODEL OF NUCLEAR FUSION

Precision experiments performed in recent years to measure the energy dependence of the cross section for near-barrier fusion make it possible to estimate quite accurately the second derivative of $E\sigma_{\text{fus}}(E)$ with respect to energy. In the classical limit, this derivative can be identified with the distribution with respect to barriers [19],

$$D(B) = \frac{1}{\pi R_B^2} d^2(E\sigma_{\text{fus}})/dE^2|_{E=B}. \quad (26)$$

The discovery of a rather complicated structure of the function $D(B)$ in the near-barrier region of energies [2–4] (this structure is different for different combinations of nuclei) was the main net result of such measurements. This is indicative of a nontrivial dynamics of passage through the potential barrier under conditions of strong channel coupling.

In the absence of channel coupling (this corresponds to the disregard of all degrees of freedom, with the exception of that which is associated with the relative motion of spherical nuclei), the effective interaction potential

$$V_{\text{eff}}(r) = V(r) + \frac{\hbar^2}{2\mu}\frac{l(l+1)}{r^2}$$

can be approximated near its maximum by an "inverted" parabola,

$$V_{\text{eff}}(r) \approx B(l) + 1/2V''(r)|_{r=R_B}[r - R_B(l)]^2.$$

In this case, the barrier penetrability is determined by the well-known Hill–Wheeler formula [20]

$$T(l,E) = \left[1 + \exp\left(\frac{2\pi}{\hbar\omega_B}[B(l) - E]\right)\right]^{-1}, \quad (27)$$

where $B(l)$ and $R_B(l)$ are the barrier height and position, respectively, and $\omega_B(l) = \sqrt{-V''(R_B)/\mu}$ is the oscillator frequency, which characterizes the barrier

width and which, in general, depends on the energy E. If we now assume that the effective-barrier position $R_B(l)$ changes only slightly in response to a change in l, the barrier height is given by

$$B(l) = B + \frac{\hbar^2}{2\mu R_B^2} l(l+1),$$

where B and R_B are, respectively, the barrier height and position at $l = 0$. In this case, the barrier penetrability $T(l, E)$ does not depend on B and l independently, but it is a function of the combination

$$x = B + \frac{\hbar^2}{2\mu R_B^2} l(l+1) - E;$$

that is, $T(l, E) = f(x)$. By using expression (20) for the fusion cross section, we arrive at

$$\frac{d(E\sigma_{\text{fus}})}{dE} = \frac{\pi\hbar^2}{2\mu} \sum_{l=0}^{\infty} (2l+1) \frac{dT(l,E)}{dE}. \qquad (28)$$

Since

$$\frac{dT}{dE} = -\frac{dT}{dx} = -\frac{dT}{dl}\left(\frac{dx}{dl}\right)^{-1} = -\frac{dT}{dl}\frac{2\mu R_B^2}{\hbar^2}\frac{1}{2l+1},$$

we have

$$\frac{d(E\sigma_{\text{fus}})}{dE} = -\pi R_B^2 \sum_{l=0}^{\infty} \frac{dT(l,E)}{dl}.$$

In a collision of heavy nuclei, in which case the cross section receives large contributions from many partial waves, $T(l, E)$ is a smooth function of l, so that the sum in (28) can be replaced by an integral with respect to l. This integral can be readily evaluated. The result is $d(E\sigma_{\text{fus}})/dE = \pi R_B^2 T(l = 0, E)$ or

$$D(E) = \frac{1}{\pi R_B^2}\frac{d^2(E\sigma_{\text{fus}})}{dE^2} = \frac{dT(l=0,E)}{dE}. \qquad (29)$$

In the classical case, $T(E) = 1$ for $E > B$ and $T(E) = 0$ for $E < B$; that is, $D(E) = \delta(E - B)$. In the quantum case, the penetrability of a one-dimensional barrier has the form (27) and the function $D(E)$ has one maximum at $E = B$, its width being $\Delta_B = \hbar\omega_B \ln(17 + 12\sqrt{2})/2\pi \approx 0.56\hbar\omega_B$ (for a parabolic barrier).

In a realistic case, the potential of nucleus–nucleus interaction is a multidimensional function (see Fig. 2), so that the incident flux overcomes the Coulomb barrier at different points—that is, at different values of B [this corresponds to different values of the dynamical deformation or (and) different orientations of the nuclei]. In order to obtain a simple estimate of the penetrability of such a multidimensional barrier, a semiempirical formula was proposed in [17] on the basis of a parametrized distribution with respect to barriers. Within this approach, the total penetrability is averaged over the barrier height B. Instead of (27), we then have

$$T(l,E) = \int F(B)\left[1 + \exp\left(\frac{2\pi}{\hbar\omega_B}\right.\right. \qquad (30)$$
$$\left.\left. \times \left[B + \frac{\hbar^2}{2\mu R_B^2(l)} l(l+1) - E\right]\right)\right]^{-1} dB,$$

where the function $F(B)$ satisfies the normalization condition $\int F(B)dB = 1$. It can be approximated by a symmetric Gaussian function having the center at $B_0 = (B_1 + B_2)/2$ and the width $\Delta_B = (B_2 - B_1)/2$. For statically deformed nuclei, the quantities B_1 and B_2 are defined as the barriers of the "nose-to-nose" and "side-to-side" configurations (see Fig. 2*a*), which are two limiting configurations. In this case, one can also employ a direct averaging over nuclear orientations, determining the actual barrier $B(\boldsymbol{\beta}_1, \theta_1; \boldsymbol{\beta}_2, \theta_2)$. For nuclei of zero static deformation, B_1 corresponds to the minimum height of the multidimensional barrier with allowance for a dynamical deformation (saddle point in Fig. 2*b*), while B_2 corresponds to the barrier in the case of the interaction of spherical nuclei. Our experience showed that, in order to describe more accurately the cross section for the fusion of heavy nuclei, in which case the difference $(B_2 - B_1)$ is great, it would be better to approximate the function $F(B)$ by a slightly asymmetric Gaussian function having a smaller "intrinsic" half-width (at smaller values of B) [17].

5. FUSION CROSS SECTIONS IN THE PRESENCE OF STRONG CHANNEL COUPLING

In order to compare the results of our calculations for the nuclear-fusion cross sections not only with experimental data but also with the results of the calculations based on the CCFULL code [6], we employ here the Woods–Saxon potential for nucleus–nucleus interaction since the CCFULL code is unable to operate with the proximity potential.

In calculating the cross section for the fusion of a ^{16}O nucleus with a deformed nucleus ^{154}Sm, we set the parameters involved to the following values: $V_0 = -105$ MeV, $r_0^V = 1.12$ fm, $a_V = 0.75$ fm (see Fig. 2*a*), $r_0^1 = 1.2$ fm, and $r_0^2 = 1.06$ fm; also, we took the values of $\beta_2 = 0.3$ and $\beta_4 = 0.1$ for the parameters of, respectively, the static quadrupole and the static hexadecapole deformation of the ^{154}Sm nucleus and the value of $E_{2^+} = 0.084$ MeV for the energy of the first excited rotational level; in addition, we used the values of $R_{\max} = 24$ fm and $h = 0.05$ fm. The fusion cross

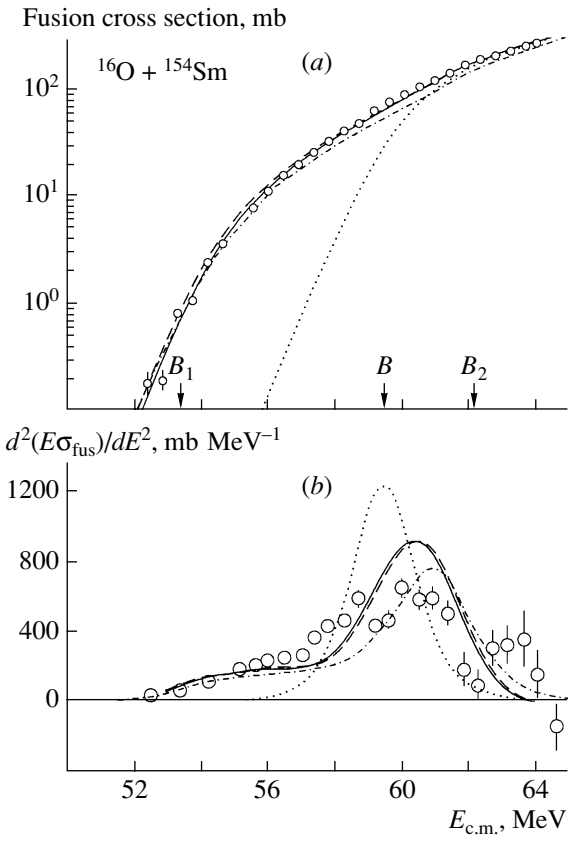

Fig. 3. (*a*) Cross section for the fusion of oxygen nuclei with a deformed nucleus ^{154}Sm and (*b*) distribution with respect to barriers. The dotted curves correspond to the fusion of spherical nuclei. The dashed and solid curves represent the results of the calculations by, respectively, the CCFULL code [6] and our code with allowance for five rotational states of the ^{154}Sm nucleus. The dash-dotted curve for the cross section was obtained by a mere averaging over the orientations of the deformed nucleus. The displayed experimental data were borrowed from [21]. The arrows indicate the positions of the Coulomb barriers for spherical nuclei and for two limiting orientations of the deformed target nucleus.

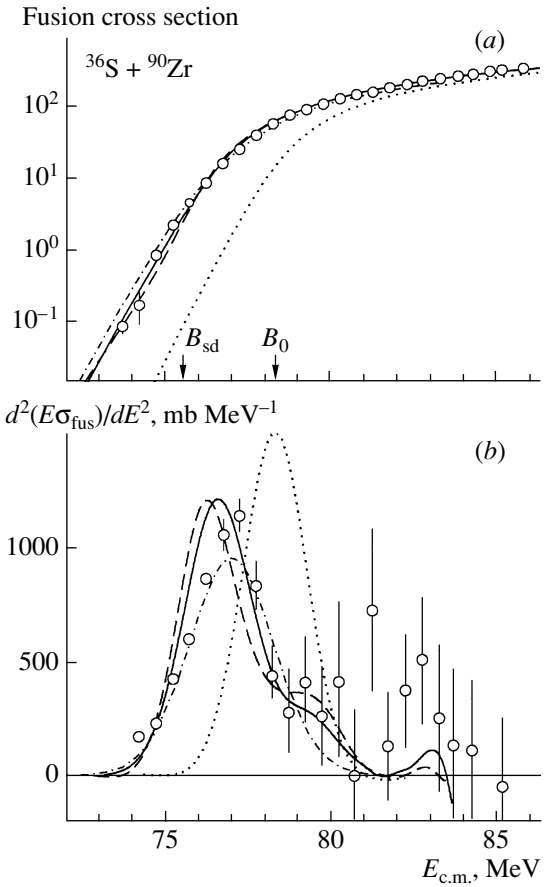

Fig. 4. (*a*) Cross section for the fusion of spherical nuclei ^{36}S and ^{90}Zr and (*b*) distribution with respect to barriers. The dotted curves correspond to the calculation that disregards dynamical deformations. The dashed and solid curves represent the results of the calculations by, respectively, the CCFULL code [6] and our code with allowance for the excitation of four phonons associated with octupole vibrations of the surface of the ^{90}Zr nucleus. The dash-dotted curve for the cross section was calculated on the basis of an empirical model for taking into account dynamical deformations (see main body of the text). The displayed experimental data were borrowed from [22].

sections calculated with allowance for the excitation of five rotational states by using our code and the CCFULL code are displayed in Fig. 3*a* along with experimental data borrowed from [21]. Figure 3*b* shows the distribution with respect to barriers, $d^2(E\sigma_{\text{fus}})/dE^2$, which makes it possible to visualize in greater detail the "fine structure" and the complicated character of barrier penetrability. As can be seen from Fig. 3, the two codes in question lead to nearly identical values for the reaction being considered. It should be noted that, for the fusion of deformed nuclei, a correct choice of internuclear interaction potential in combination with a mere averaging of one-dimensional barrier penetrabilities over the orientations of the nuclei involved (as a matter of fact, over barrier heights—see Fig. 2*a*) leads to quite satisfactory agreement with experimental data both in what is concerned with the magnitude of the fusion cross sections in the subbarrier region and in what is concerned with the shape of the distribution with respect to barriers.

The cross sections for the fusion of spherical nuclei ^{36}S and ^{90}Zr are shown in Fig. 4*a* according to calculations that take into account four phonons associated with octupole vibrations of the surface of the ^{90}Zr nucleus ($\lambda = 3$, $\hbar\omega_\lambda = 2.75$ MeV, $\langle\beta_\lambda^0\rangle = 0.22$). The corresponding distributions with respect to barriers are given in Fig. 4*b*. The displayed experimental data were borrowed from [22]. For this case, the nucleus–nucleus interaction of spherical nuclei was also cho-

sen in the form of the Woods–Saxon potential, its depth, range, and diffuseness parameter being set to $V_0 = -77.5$ MeV, $r_0^V = 1.15$ fm, and $a_V = 0.8$ fm, respectively. This potential leads to the Coulomb barrier height of $B_0 = 78.3$ MeV (right arrow in Fig. 4*a*). Upon taking into account the octupole vibrations of the target nucleus, the fusion cross section becomes much larger in the subbarrier region, the two codes in question (CCFULL [6] and our code) yielding very close results.

An increase in the fusion cross section in the subbarrier region $E < B_0$ can easily be explained with the aid of the data in Fig. 2*b*. For the case of a prolate configuration (positive values of β_λ), a dynamical deformation of the surface leads to the lowering of the Coulomb barrier. As the deformation increases further, the potential energy increases again because of a nonzero stiffness C_λ of the nuclear surface. Thus, we see that, in the total nucleus–nucleus potential, we can single out the saddle point $(r_{\rm sd}, \beta_{\rm sd})$ corresponding to the minimum height $B_{\rm sd}$ of the Coulomb barrier in the (r, β) space (see Fig. 2*b*). Using the experimental value of the energy of the photon associated with octupole vibrations of the ^{90}Zr nucleus ($\hbar\omega_{\lambda=3} = 2.75$ MeV), calculating the stiffness of the corresponding oscillator (see Section 1), and constructing the two-dimensional surface of nucleus–nucleus interaction (similar to that which is shown in Fig. 2*b*), we can easily determine, for this case, the height of the Coulomb barrier at the saddle point, $B_{\rm sd} = 75.6$ MeV (right arrow in Fig. 4*a*). Assuming that the incident flux, moving in the (r, β) space, traverses the two-dimensional barrier at various values of the dynamical deformation in the range $0 \le \beta < \beta_{\rm sd}$, we can approximate the distribution with respect to barriers by a Gaussian function having a center at the point $(B_0 + B_{\rm sd})/2$ and the half-width $(B_0 - B_{\rm sd})/2$ and calculate thereupon the total fusion cross section. The cross section obtained on the basis of this semiempirical approach is in rather satisfactory agreement both with experimental data and with the results of our precise calculations (see dash-dotted curves in Fig. 4), furnishing, at the same time, quite a clear explanation for an increase in the subbarier penetrability and in the width of the distribution with respect to barriers.

The data in Fig. 5, which shows the squared modulus of the two-dimensional wave function describing the relative motion of ^{36}S and ^{90}Zr nuclei in $(r, s_{\lambda=3})$ space, where $s_{\lambda=3} = \sqrt{(2\lambda+1)/4\pi}R_0\beta_{\lambda=3}$ is the absolute value of the octupole deformation of the ^{90}Zr nucleus, provides an additional piece of evidence in support of this qualitative pattern. It can be seen that, at large distances, the multichannel wave function is concentrated in the region of small deformations,

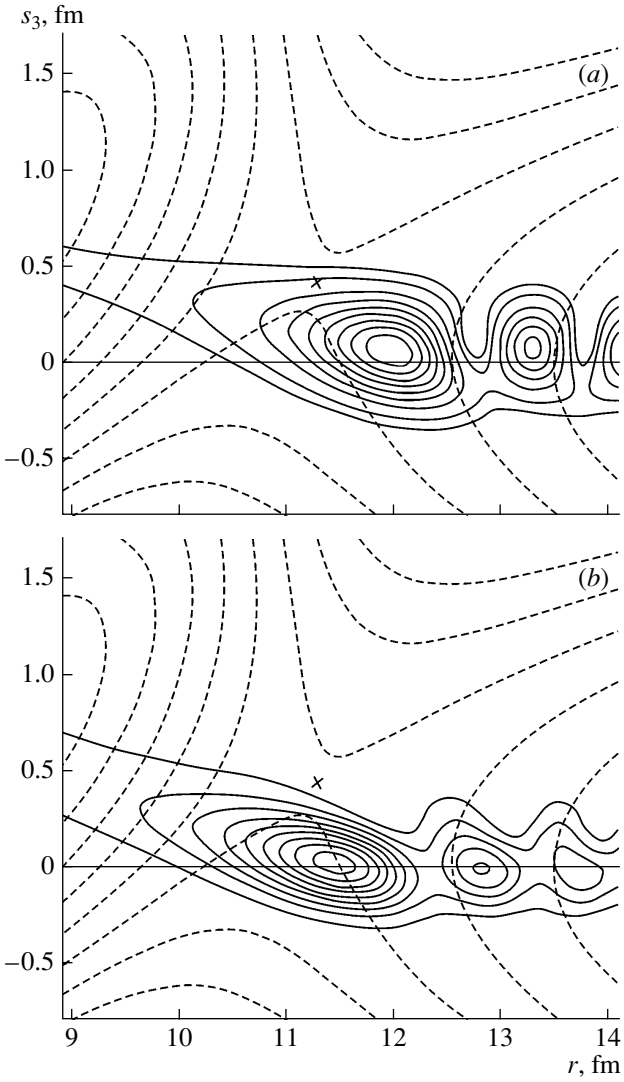

Fig. 5. Topographical landscape of the squared modulus of the two-dimensional wave function (13) (solid curves), which describes the fusion of ^{36}S and ^{90}Zr nuclei at $l = 0$, against the background of the landscape of the potential energy (dashed curves) at energies of $E_{\rm c.m.} =$ (*a*) 77 and (*b*) 80 MeV. The cross indicates the position of the saddle point of the Coulomb barrier.

$\beta_3 \approx 0$, this reflecting the dominance of zero-point vibrations of the nuclear ground state $\varphi_{\nu=0}(\beta)$ in the expansion given by (13). At low energies (slow collisions), the nuclei involved undergo considerable deformations at the instant of coming into contact, the Coulomb barrier being overcome predominantly at positive values of the deformation (the stretching of the nuclei toward each other), which lead to the lowering of this barrier (see Fig. 2*a* and the landscape of the potential energy in Fig. 5). That the modulus of the wave function oscillates at large distances is due to the interference between the incident and the reflected wave.

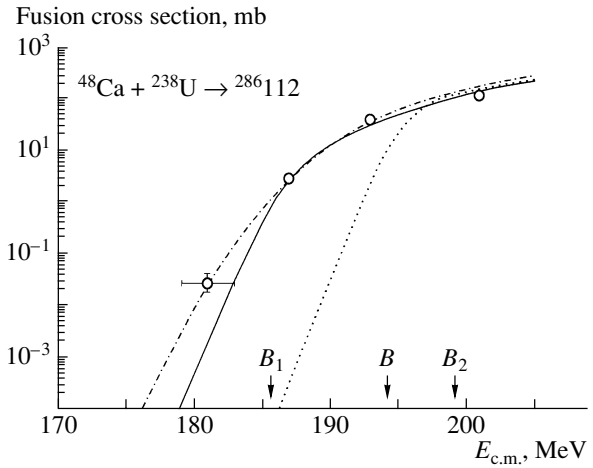

Fig. 6. Cross section for the fusion of a ^{48}Ca nucleus and a deformed ^{238}U nucleus: (dotted curve) fusion of spherical nuclei, (solid curve) results of the calculation by the coupled-channel method with the aid of the algorithm proposed in the present study, (dash-dotted curve) cross section obtained within the semiempirical approach, and (points) experimental data borrowed from [23]. The arrows indicate the positions of the Coulomb barriers for spherical nuclei (Bass barrier) and for two limiting configurations of the deformed target nucleus.

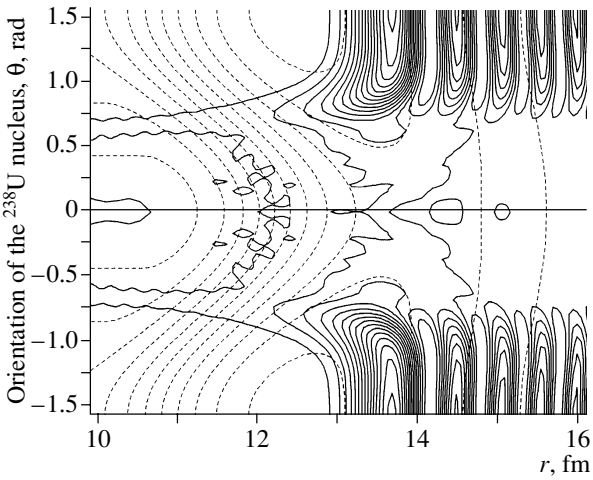

Fig. 7. Topographical landscape of the squared modulus of the two-dimensional wave function (13) at $l = 0$ (solid curves), which describes the fusion of ^{48}Ca and ^{238}U nuclei at an energy of $E_{c.m.} = 194$ MeV, against the background of the landscape of the potential energy (dashed curves).

6. SYNTHESIS OF SUPERHEAVY NUCLEI

In the fusion of very heavy nuclei, which are used, in particular, in the synthesis of superheavy elements, the coupling of channels plays an even more significant role. For this region of nuclei, available experimental data on fusion cross sections are much scarcer; moreover, no experimental data for nuclear combinations close to symmetric ones can be obtained in principle because it is impossible, in this case, to separate products originating from processes of deep-inelastic scattering, on one hand, and from the fission of a compound nucleus, on the other hand. In view of this, theoretical calculations and predictions are of paramount importance in this region of nuclei. The reliability of such predictions is not very high at the present time not only because of problems encountered in taking into account the coupling of several degrees of freedom in the process of near-barrier fusion but also because of inaccuracies in determining the nucleus–nucleus interaction. Until recently, there has been no possibility for performing quantum calculations of the fusion of very heavy nuclei within the coupled-channel method, because the operation of the existing algorithms (including the CCFULL code) is highly unstable in this case. It turned out that our new algorithm for solving a set of a large number of coupled equations makes it possible to perform such calculations.

Figure 6 shows the experimental and theoretical cross sections for the fusion of ^{48}Ca and ^{238}U nuclei. The displayed experimental data, which were taken from [23], correspond to all products of fission (both ordinary fission and prompt fission proceeding without the formation of a compound nucleus); therefore, it is more correct, in this case, to refer to this quantity as the capture cross section (see the comment at the end of Section 2). For the nuclear interaction, we again took the Woods–Saxon potential with parameters $V_0 = -160$ MeV, $r_0^V = 1.14$ fm, and $a_V = 0.65$ fm, which ensure the Coulomb barrier height of $B = 194$ MeV, predicted by the Bass model [24] for these nuclei. The static quadrupole deformation of $\beta_2 = 0.215$ [25], which is realized for the ^{238}U nucleus, leads to the barrier heights of $B_1 = 185.4$ MeV and $B_2 = 199.2$ MeV for two limiting orientations of the nuclei. Employing the semiempirical model of nuclear fusion and approximating the function $F(B)$ in (30) by an asymmetric Gaussian function whose width is $\Delta_B^1 = (B_2 - B_1)/2 \approx 7$ MeV for the right branch (large values of B) and $\Delta_B^2 = 5$ MeV for the left branch (as a matter of fact, this is an adjustable parameter here), we have also obtained quite satisfactory agreement with experimental data (dash-dotted curve in Fig. 6).

The squared modulus of the two-dimensional wave function describing the relative motion of ^{48}Ca and ^{238}U nuclei is shown in Fig. 7 versus the distance r and the angle θ of rotation of the deformed uranium nucleus. For the interaction of these two nuclei, Fig. 7 also displays the potential-energy landscape, which is similar to that in Fig. 2*a*. The value chosen for the collision energy, $E_{c.m.} = 194$ MeV, is above the

Coulomb barrier height at $\theta = 0°$ (about 185 MeV) and below this barrier at $\theta = \pi/2$ (about 200 MeV). As can be seen from the figure, the incident wave therefore overcomes the barrier almost freely only at small θ (in the nose-to-nose configuration), but it is almost completely reflected from the barrier at $\theta \sim \pi/2$. At large distances, this leads to a strong interference between the incident and the reflected wave at $\theta \sim \pi/2$ and to an almost complete absence of interference at small θ.

In conclusion, we note that the algorithms developed by us for calculating the cross sections for the near-barrier fusion of heavy nuclei (coupled-channel method and semiempirical model) and used in the present study can be found, together with the code for computing multidimensional potential surfaces, on the freely accessible Web server quoted in [26].

ACKNOWLEDGMENTS

This work was supported in part by the Russian Foundation for Basic Research (project no. 03-07-90373).

APPENDIX 1

Local Curvature of the Surface of a Deformed Nucleus and Geometric Factor

In terms of polar coordinates, the local curvature of a curve in a plane can be represented as [11, formula (17.1-9)]

$$k = \left[\rho^2 + 2\left(\frac{d\rho}{d\varphi}\right)^2 - \rho\frac{d^2\rho}{d\varphi^2}\right]\left[\rho^2 + \left(\frac{d\rho}{d\varphi}\right)^2\right]^{-3/2}. \quad (A.1)$$

In the case of dynamical deformations along the common symmetry axis of the nuclei (nose-to-nose orientation), any curve lying on the surface of a nucleus in a plane containing the symmetry axis is given by (1); that is, $\rho(\varphi) \equiv R(\theta)$. At small angles ($\theta \ll 1$), we can use an approximate expression for Legendre polynomials,

$$P_\lambda(\cos\theta) \approx 1 - \eta(\lambda)(1 - \cos\theta), \quad \theta \ll 1,$$

where $\eta(\lambda) = 3 \cdot 4 \cdots (\lambda + 1)/(\lambda - 1)!$, whereupon the equation of the surface takes the form

$$R(\theta) = a + b\cos\theta, \quad (A.2)$$

$$a = \tilde{R}\left[1 + \sum_{\lambda\geq 2}\beta_\lambda\left(1 - \eta(\lambda)\right)\sqrt{\frac{2\lambda+1}{4\pi}}\right],$$

$$b = \tilde{R}\left[1 + \sum_{\lambda\geq 2}\beta_\lambda\eta(\lambda)\sqrt{\frac{2\lambda+1}{4\pi}}\right].$$

At $\theta = 0$, the substitution of (A.2) into (A.1) yields

$$k^\perp = k^{||} = k = \frac{a + 2b}{(a+b)^2}, \quad (A.3)$$

$$k = \tilde{R}^{-1}\left(1 + \sum_{\lambda\geq 2}\sqrt{\frac{2\lambda+1}{4\pi}}\beta_\lambda\right)^{-2} \times \left(1 + \sum_{\lambda\geq 2}(1 + \eta(\lambda))\sqrt{\frac{2\lambda+1}{4\pi}}\beta_\lambda\right), \quad (A.4)$$

whence we obtain formula (7).

In the case of statically deformed nuclei rotating in the reaction plane, a calculation of a local curvature for an arbitrary orientation of the symmetry axes of the nuclei leads to more cumbersome formulas. A simple expression is obtained for the limiting case of $\theta = \pi/2$ (side-to-side configuration). Since a static quadrupole deformation is the most peculiar to nuclei, we consider here only the case of $\lambda = 2$. Using the expression $(3\cos 2\theta + 1)/4$ for the Legendre polynomial $P_2(\cos\theta)$, we obtain

$$R(\theta) = a' + b'\cos 2\theta, \quad (A.5)$$

where

$$a' = \tilde{R}\left[1 + \frac{1}{4}\beta_2\sqrt{\frac{5}{4\pi}}\right], \quad b' = \frac{3}{4}\tilde{R}\beta_2\sqrt{\frac{5}{4\pi}}.$$

The substitution of (A.5) into (A.1) at $\theta = \pi/2$ yields

$$k^{||} = \frac{a' - 5b'}{(a' - b')^2} = \frac{R_A}{R_B^2}, \quad k^\perp = \frac{1}{R_B} \quad (A.6)$$

where

$$R_A = \tilde{R}\left[1 - \frac{7}{2}\beta_2\sqrt{\frac{5}{4\pi}}\right],$$

$$R_B = R(\theta = \pi/2) = \tilde{R}\left[1 - \frac{1}{2}\beta_2\sqrt{\frac{5}{4\pi}}\right].$$

A further calculation of the local geometric factor $G_{\mathrm{loc}} = P_{\mathrm{sph}}/P$ is performed with the aid of formula (6), which, as was mentioned above, leads to a singularity when two planar surfaces touch each other [$k_1^\perp + k_2^\perp = 0$ or (and) $k_1^{||} + k_2^{||} = 0$].

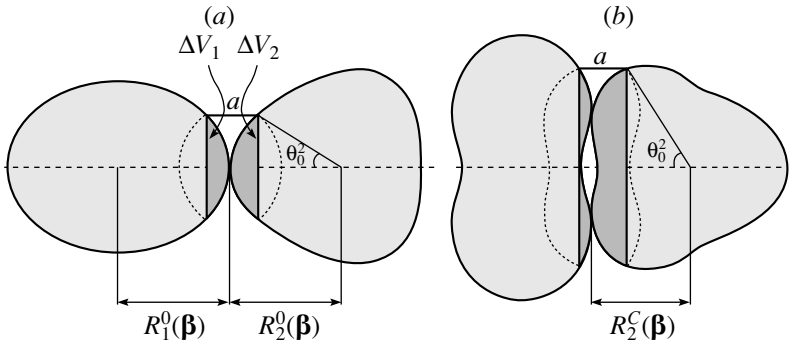

Fig. 8. Schematic representation of two deformed nuclei in the nose-to-nose configuration (the horizontal dashed line is the symmetry axis): (*a*) positive deformations and (*b*) negative deformations. More darkly shaded segments are regions that make a dominant contribution to nucleus–nucleus interaction.

APPENDIX 2

Geometric Factor with Allowance for the Finiteness of the Range of Nuclear Forces and Dimensions of Deformed Nuclei

In principle, a precise value of the geometric factor can be obtained by using the folding procedure for calculating the potential for the nucleus–nucleus interaction. In this case, the finiteness of nuclear sizes and of the range of nucleon–nucleon interaction guarantees the absence of singularities even in the case of zero local curvature at the point where the nuclear surfaces touch each other. In specific applications (especially in dynamical calculations), however, it is more convenient to use, instead of folding potentials, some analytic expression (like the Woods–Saxon potential or the proximity potential) that would represent the nucleus–nucleus interaction and which would take into account the change in the curvature of nuclear surfaces at large deformations. An approximate value of the geometric factor can be obtained with the aid of the expression

$$G = \frac{\Delta V_1(\boldsymbol{\beta}_1, \theta_1; a_1) + \Delta V_2(\boldsymbol{\beta}_2, \theta_2; a_2)}{\Delta V_1^0(a_1) + \Delta V_2^0(a_2)}, \qquad \text{(A.7)}$$

where $\Delta V_i(\boldsymbol{\beta}_i, \theta_i; a_i)$ are the volumes of the most closely spaced small segments of the nuclei being considered (see Fig. 8), $\Delta V_i^0(a_i) = (\pi/3)a_i^2(3R - a_i)$ are the volumes of the segments of the corresponding spherical nuclei, $a_1/a_2 = (R_2 - a/2)/(R_1 - a/2)$, and $a \approx 1$ fm. We will first consider the deformation along the common symmetry axis of the nuclei (Fig. 8*a*). In this case, the volume of the nose segment is given by

$$\Delta V_i = \frac{2\pi}{3}\tilde{R}_i^3 \int\limits_{t_0^i}^{1} \left[1 + \sum_\lambda \beta_{i\lambda}\sqrt{\frac{2\lambda+1}{4\pi}}P_\lambda(t)\right]^3 dt$$
$$- \frac{\pi}{3}(R_i^0 - a_i)^3(1/t_0^{i^2} - 1), \qquad \text{(A.8)}$$

where $R_i^0 = R_i(\boldsymbol{\beta}_i, \theta = 0)$ and t_0^i is found from the equation ($t \equiv \cos\theta$)

$$R(t)t = R_i^0 - a_i. \qquad \text{(A.9)}$$

This equation can be solved explicitly if a parabolic approximation of Legendre polynomials is used in the range $0 < t \leq 1$; that is,

$$P_\lambda(t) \approx -p_\lambda + \alpha_\lambda(t - \tau_\lambda)^2, \qquad \text{(A.10)}$$

where $p_\lambda = \{1/2, \sqrt{1/5}, 3/7\}$, $\tau_\lambda = \{0, \sqrt{1/5}, \sqrt{3/7}\}$, and $\alpha_\lambda = (1 + p_\lambda)/(1 - \tau_\lambda)^2$ at $\lambda = 2$, 3, and 4, respectively. In this case, Eq. (A.9) is a cubic equation, and we must take the positive root of this equation for t_0^i. Integration in (A.8) can also be performed explicitly. For the volume of the nose segment of a deformed nucleus, this yields a rather cumbersome expression, but it is readily calculable. Obviously, the geometric factor (A.7) does not have singularities, remaining finite at any deformations.

At large negative deformations, the nuclear surface at the point $\theta = 0$ first becomes flat and then assumes a concave shape (see Fig. 8*b*). In this case, the "interacting-layer" thickness a must be reckoned not from the point $R_i^0 = R_i(\boldsymbol{\beta}_i, \theta = 0)$, which lies on the symmetry axis, but from the point that lies on the surface and which is the most remote from the center of the nucleus along the axis connecting the centers of the nuclei—that is, from the point $R_i^C \equiv R_i(t_C^i)t_C^i$ in Fig. 8*b*, which is found from the condition $d[R(t)t]/dt|_{t_C} = 0$. In this case, the quantity $t_0^i \equiv \cos\theta_0^i$ is as before determined from Eq. (A.9), where R_i^0 is replaced by R_i^C. In Fig. 9, the geometric factor calculated by formula (A.7) is contrasted against the local approximation $G_{\text{loc}} = P_{\text{sph}}/P$. It can be seen that, in the region of positive and small negative deformations, the approximation of "finite segments" is

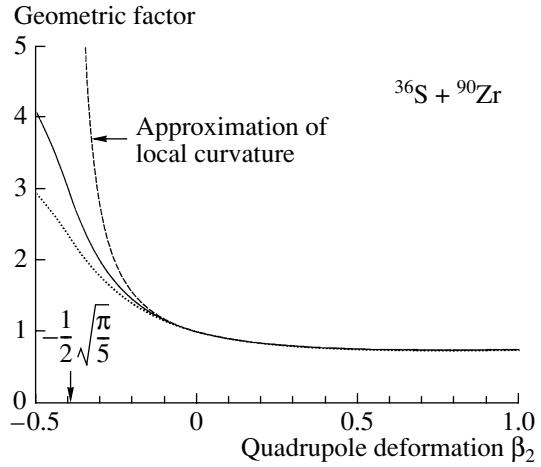

Fig. 9. Geometric factor calculated for the case of identical dynamical quadrupole deformations ($\beta_{1,2} = \beta_{2,2} = \beta_2$) of the interacting nuclei ^{36}S and ^{90}Zr. The dashed curve corresponds to the local approximation $G_{\rm loc} = P_{\rm sph}/P$. The solid and the dotted curve were calculated by formula (A.7) at $a = 1$ and 2 fm, respectively. The arrow indicates the "critical" deformation at which the local curvature of the surface featuring a quadrupole deformation vanishes (contiguity of two flat surfaces).

weakly dependent on a and is virtually coincident with the local approximation.

For rotating deformed nuclei, the volumes of the "interacting segments," $\Delta V_i(\boldsymbol{\beta}_i, \theta_i; a_i)$, depend on the orientation of the symmetry axes of the nuclei. As was indicated above, a static quadrupole deformation is the most peculiar to nuclei—that is, $\beta_{3,4}^{\rm g.s.} \ll \beta_2^{\rm g.s.}$. In addition, we note that, at $a \approx 1$ fm, the deviation of the volumes $\Delta V_i(\boldsymbol{\beta}_i, \theta_i; a_i)$ from the spherical ones is much less for higher multipole orders than for $\lambda = 2$. In calculating the angular dependence of the geometric factor, one can therefore take into account only static quadrupole deformations of interacting nuclei. In order to calculate the volume of the side segment of a nucleus (side-to-side orientation of nuclei—that is, $\theta_i = \pi/2$), we can again use formula (A.9) to find the angle θ_0^i ($t_0^i \equiv \cos\theta_0^i$) of the corresponding cone. In this formula, however, we must replace $R_i^0 = R_i(\boldsymbol{\beta}_i, \theta = 0)$ by $R_i^B = R_i(\boldsymbol{\beta}_i, \theta = \pi/2)$. In this case, the base of the segment is an ellipse whose semiaxes are $A = \sqrt{2R_i^B a_i - a_i^2}$ and $B = (R_i^B - a_i)/\tan\theta_0^i$, its volume being approximately

$$\Delta V_i = \frac{\pi}{2} a_i^2 \sqrt{2R_i^B - a_i}(R_i^B - a_i)/\tan\theta_0^i. \quad \text{(A.11)}$$

Knowing the volumes of the surface segments for the two limiting orientations—ΔV_i^N calculated by formula (A.8) at $\theta_i = 0$ and ΔV_i^S calculated by formula (A.11) at $\theta_i = \pi/2$—one can approximate the volume of the segment of an arbitrarily rotated nucleus by the simple expression $\Delta V_i(\theta_i) = 0.5(\Delta V_i^S + \Delta V_i^N) - 0.5(\Delta V_i^S - \Delta V_i^N)\cos 2\theta_i$ and then use formula (A.7) to calculate the geometric factor in the potential of the interaction of two deformed nuclei arbitrarily rotated in the reaction plane.

REFERENCES

1. M. Beckerman, Rep. Prog. Phys. **51**, 1047 (1988), and references therein.
2. *Heavy Ion Fusion*, Ed. by A. M. Stefanini *et al.* (World Sci., Singapore, 1994).
3. *Papers from Fusion 97*, J. Phys. G **23**, 1157 (1997).
4. M. Dasgupta, D. J. Hinde, N. Rowley, and A. M. Stefanini, Annu. Rev. Nucl. Part. Sci. **48**, 401 (1998).
5. C. H. Dasso and S. Landowne, Comput. Phys. Commun. **46**, 187 (1987); J. Fernandez-Niello, C. H. Dasso, and S. Landowne, Comput. Phys. Commun. **54**, 409 (1989).
6. K. Hagino, N. Rowley, and A. T. Kruppa, Comput. Phys. Commun. **123**, 143 (1999).
7. V. I. Zagrebaev, N. S. Nikolaev, and V. V. Samarin, Izv. Akad. Nauk, Ser. Fiz. **61**, 2157 (1997).
8. N. Takigawa, T. Rumin, and N. Ihara, Phys. Rev. C **61**, 044607 (2000).
9. J. Blocki, J. Randrup, W. J. Swiatecki, and C. F. Tsang, Ann. Phys. (N.Y.) **105**, 427 (1977).
10. R. A. Broglia, C. H. Dasso, and A. Winter, in *Proceedings of the International School of Physics "Enrico Fermi," Course LXXVII, Varenna, 1979*, Ed. by R. A. Broglia, R. A. Ricci, and H. A. Dasso (North-Holland, Amsterdam, 1981), p. 327.
11. G. A. Korn and T. M. Korn, *Mathematical Handbook for Scientists and Engineers* (McGraw-Hill, New York, 1961; Nauka, Moscow, 1971).
12. I. I. Gontchar, M. Dasgupta, D. J. Hinde, *et al.*, Phys. Rev. C **65**, 034610 (2002).
13. A. Bohr and B. R. Mottelson, *Nuclear Structure,* Vol. 2: *Nuclear Deformations* (Benjamin, New York, 1975; Mir, Moscow, 1977), Vol. 2.
14. M. A. Nagarajan, N. Rowley, and R. J. Lindsay, J. Phys. G **12**, 529 (1986).
15. J. H. Wilkinson and C. Reinsch, *Linear Algebra* (Springer-Verlag, Berlin, 1971; Mashinostroenie, Moscow, 1976).
16. J. Tôke, R. Bock, G. X. Dai, *et al.*, Nucl. Phys. A **440**, 327 (1985).
17. V. I. Zagrebaev, Phys. Rev. C **64**, 034606 (2001).
18. *Modern Numerical Methods for Ordinary Differential Equations,* Ed. by G. Hall and J. Watt (Oxford Univ. Press, Oxford, 1976; Mir, Moscow, 1979).
19. N. Rowley, G. R. Satchler, and P. H. Stelson, Phys. Lett. B **254**, 25 (1991).
20. D. L. Hill and J. A. Wheeler, Phys. Rev. **89**, 1102 (1953).
21. J. R. Leigh *et al.*, Phys. Rev. C **52**, 3151 (1995).

22. F. Scarlassara, S. Beghini, G. Montagnoli, *et al.*, in *Proceedings of the International Workshop on Fusion Dynamics at the Extremes, Dubna, 2000*, Ed. by Yu. Ts. Oganessian and V. I. Zagrebaev (World Sci., Singapore, 2001), p. 274.
23. M. G. Itkis *et al.*, in *Proceedings of the International Workshop on Fusion Dynamics at the Extremes*, Dubna, 2000, Ed. by Yu. Ts. Oganessian and V. I. Zagrebaev (World Sci., Singapore, 2001), p. 93.
24. R. Bass, *Nuclear Reactions with Heavy Ions* (Springer-Verlag, Berlin, 1980), p. 326.
25. P. Möller, J. R. Nix, W. D. Myers, and W. J. Swiatecki, At. Data Nucl. Data Tables **59**, 185 (1995).
26. http://nrv.jinr.ru/nrv/.

Translated by A. Isaakyan